Spatial Inductance Estimation for Current Loop Auto-Tuning in IPMSM Self-Commissioning

Feyzullah Erturk and Bilal Akin, *Senior Member, IEEE*

***Abstract*—This paper presents a comprehensive study on current loop auto-tuning for self-commissioning of sensorless interior permanent magnet synchronous machine (IPMSM) drives. Well-tuned current controllers are essential for both high-performance operation and self-commissioning procedure. However, current controller design parameters, i.e., L_d and L_q, are not known at the beginning of the self-commissioning procedure where their estimation also has unique challenges. For example, an initial rotor position to determine the actual *d*- and *q*-axes is not known. Also, feedback controllers cannot be used in the estimation because they are not tuned yet. As a solution, this paper proposes a method to estimate the spatial inductance map by spatially scanning the motor via sinusoidal voltage injection in a controlled manner. Then it uses the estimated inductance values to tune the current controllers. The proposed method identifies L_d and L_q values using open-loop voltage injection without needing actual *d*- and *q*-axis positions. The whole procedure takes around a second. Practical considerations such as an automatic selection of the injection voltage, and digital control and dead-time effects are carefully addressed. The findings are experimentally verified on a 3-phase IPMSM drive. Furthermore, its applicability to different motor types is also demonstrated.**

***Index Terms*—Auto-tuning, current controller, inductance estimation, interior permanent magnet synchronous machine (IPMSM), self-commissioning.**

NOMENCLATURE

V_i	Injection voltage amplitude.
V_{i0}	Initialization value for V_i (design value).
$V_{\lim}$	Maximum assignable value for V_i (design value).
f_i	Injection frequency.
f_{i0}	Initialization value for f_i (design value).
$f_{\lim}$	Minimum assignable value for f_i (design value).
θ_r	Initial rotor position.
θ_e	Spatial angle for injection and inductance estimation.
$\Delta\theta_e$	Increment angle to θ_e (design value).
$L(\theta_e)$	Motor spatial inductance value at the angle of θ_e.
V_γ	γ-axis voltage reference amplitude at injection frequency.
I_γ	γ-axis current feedback amplitude at injection frequency.
α_v	Phase of γ-axis voltage reference.
α_i	Phase of γ-axis current feedback.
$I_{\min}$	Minimum value for I_γ to begin estimation.
$I_{\max}$	Maximum value for I_γ to begin estimation.
$V_{s\min}$	Lower voltage search limit.
$V_{s\min}$ Flag	Boolean value set to "True" after $V_{s\min}$ is determined.
$V_{s\max}$	Uppper voltage search limit.
$V_{s\max}$ Flag	Boolean value set to 'True' after $V_{s\max}$ is determined.

Manuscript received November 21, 2018; revised February 26, 2019 and March 31, 2019; accepted April 12, 2019. Date of publication May 8, 2019; date of current version January 3, 2020. This work was supported by Nidec Corporation and Texas Instruments Inc. *(Corresponding author: Bilal Akin.)*

The authors are with the Department of Electrical Engineering, University of Texas at Dallas, Richardson, TX 75080 USA (e-mail: feyzullah.erturk@utdallas.edu; bilal.akin@utdallas.edu).

Color versions of one or more of the figures in this paper are available online at http://ieeexplore.ieee.org

Digital Object Identifier 10.1109/TIE.2019.2914640

I. INTRODUCTION

INTERIOR permanent magnet synchronous machine (IPMSM) has been gaining popularity in several applications due to its higher efficiency and power density. High-performance operation of IPMSM requires complicated control algorithms and corresponding motor parameter information. Nonetheless, users may not have the required skills or tools to obtain accurate motor data for optimal control. Therefore, it is necessary for commercial motor drives to have the highly accurate self-commissioning capability. The results obtained by self-commissioning are essential to design the current and speed controllers; high-frequency signal injection (HFI) based sensorless control, observer-based sensorless control, and maximum torque per ampere control.

Typical functional flow of a high-performance self-commissioning procedure is given in Fig. 1. Here, the first step is current loop auto-tuning which is necessary for the next steps of the self-commissioning as well as regular drive operation. Therefore, this paper focuses on "Step–1" in order to facilitate the other steps. The motor inductances obtained in Step–1 can also be used in the design of HFI-based sensorless control [1] which is used in initial rotor position detection [2] (Step–2) and rotational part of self-commissioning (Step–5 and –6). Stator resistance (Step–3) and inductance saturation characteristics (Step–4) are identified after the current loop is auto-tuned and d- and q-axis position is obtained at Step–1 and –2. Overall, this estimation order is devised to enable the sensorless drive finish

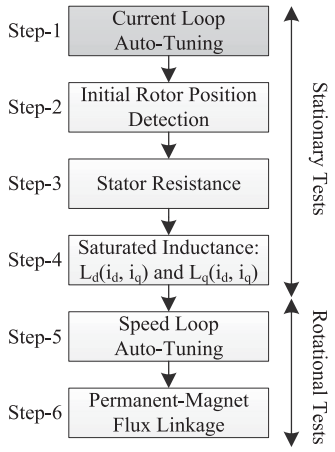

Fig. 1. Self-commissioning test sequence for IPMSM drive.

the self-commissioning with very limited initial motor data such as standard nameplate voltage, current, speed ratings, and pole number.

High-performance current controller design requires motor parameters, especially the inductances. At the very beginning, these parameters are unknown, therefore *d*- and *q*-axis inductance (L_d and L_q) should be estimated first. In the literature, several inductance estimation methods for IPMSM are proposed. In [3] and [4], recursive least squares estimator is used to identify electrical parameters of IPMSM. Initial rotor position is detected as the first step. The procedure uses the current and speed controller to force the desired identification test signals. In [5] and [6], an improved inductance estimation method is proposed considering saturation effects. It utilizes square-wave current references to ensure stationary rotor and obtain saturated inductance values. Proportional-resonance current controller is selected to track sinusoidal reference. In [7], a self-commissioning method is proposed to detect the initial rotor position and then estimate the L_d and L_q. Here, *d*-axis current controller is chosen in order to overcome the effect of inverter voltage distortion, and it is roughly tuned based on the assumptions regarding the motor parameters. The dilemma of using a current controller for inductance estimation during self-commissioning is acknowledged in [8]. Here, adaptive control theory is used to estimate the motor parameters where these estimated parameters are used in the feedforward term to relieve the burden on the current controller. Yang and Lin [9] suggests a self-commissioning method that identifies the inductances by applying voltage pulses. Here, an initial rotor position is assumed to be known. In order to improve the accuracy in such methods, it is possible to align the rotor to a known angle (e.g., zero) when identifying inductances [10]. The relay feedback based auto-tuning is proposed for IPMSM in [11]. Relay feedback causes a controlled limit cycle in the system and it is a widely used technique in the process industry [12]. Basically, this method uses the limit cycle to identify the plant model first, and then accordingly design the controller using predefined rules (e.g., Ziegler–Nichols). The limit cycle under relay feedback can only occur due to the digital control delay because the motor winding is a first-order system. Therefore, the authors of [11] use low-pass filters to reach 180° phase delay at the targeted limit-cycle frequency. In [13], a discrete Fourier transform (DFT) based inductance estimation is proposed which uses the current controller to inject test signal, and position sensor to detect the rotor position (true *d*- and *q*-axis position). However, the current controller may not be tuned and used without inductance values. Also, in practice, a solution with no position sensor is preferred. Hence, this paper proposes solutions to these practical issues and identifies L_d and L_q without using current controller and rotor position feedback.

Inductance identification for current-loop auto-tuning is challenging for a few reasons. First, as L_d and L_q may be in wide range and initially unknown, they should be identified by open-loop voltage injection rather than current injection using current controller. However, some studies cited above assume that the controllers are already tuned and they directly pass to the parameter estimation stage [3]–[6], [13]. Without known motor parameters, it is relatively hard to tune the controller and assure its stability, robustness, and bandwidth. Current controller usage before parameter identification creates a dilemma because controller tuning requires some knowledge about motor parameters. On the other hand, some studies acknowledge this dilemma and they first estimate the motor parameters in an open-loop manner or adaptively to design the controller [8]–[11]. The second reason is that the initial rotor position is not known which determines the *d*- and *q*-axis and hence the inductances at these axes. Many studies do not mention the initial position issue or assume that the initial position is known [4]–[6], [8], [9], [11], [13] whereas others use an initial rotor position detection algorithm [3], [7] or align the rotor to a known angle (e.g., zero) [10]. The initial rotor position detection may be achieved using some methods which require motor inductances [1], [2]. Therefore, similar to the current controller, employing initial position detection before parameter identification creates a dilemma because its design requires knowledge on motor inductances.

This paper proposes a simple and practical solution to estimate *d*- and *q*-axis inductances for current loop auto-tuning of an unknown motor. It offers solutions to aforementioned problems of the first step of self-commissioning. Hence, the inductance estimation is carried out by open-loop sinusoidal voltage injection. However, to be able to safely execute the procedure over many different motors, an algorithm for automatic selection of the injection amplitude and frequency is proposed. Furthermore, to rule out any initial rotor position requirement, the proposed method obtains the spatial inductance map over 180° which includes both L_d and L_q as minimum and maximum spatial inductances. The practical issues such as digital control effects and the voltage distortion due to the inverter dead-time are studied and the corresponding solutions are provided as well. The whole procedure takes around a second. Furthermore, it is experimentally verified that the proposed method can practically be employed in all ac motor types. This feature also contributes to building motor-agnostic drives, meaning that the drives can run any ac machine.

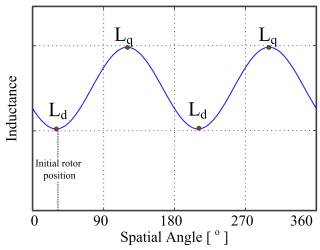

Fig. 2. Inductance dependence on rotor position in IPMSM.

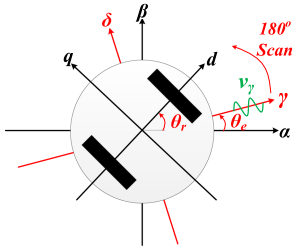

Fig. 3. Scanning voltage vector while rotor is stand-still.

II. Spatial Inductance Mapping Algorithm

Fundamentally, parameter estimation algorithms inject test voltage to the motor and observe the current response. When the current controller is used, the test voltage would automatically be determined by the controller. However, this approach is not suitable for current-loop auto-tuning in self-commissioning as discussed earlier. Therefore, this paper adopts open-loop high-frequency voltage injection with an automatic selection of test voltage whose amplitude and frequency are determined by the algorithm depicted in Fig. 6. Basically, using the amplitudes and phases of current feedback and injected voltage reference, inductances are calculated to auto-tune the current loop.

Furthermore, the inductance of IPMSMs is angle dependent as described in Fig. 2; therefore, rotor position is needed for L_d and L_q estimation. However, it is not known at the beginning. Possible solutions such as aligning the rotor to a known angle or using initial rotor position detection may not be possible in all applications. As a solution, this paper proposes spatial inductance mapping by spatially scanning the motor. The minimum inductance is assigned to L_d and the maximum inductance to L_q. Accordingly, L_d and L_q are estimated without needing initial rotor position knowledge. Voltage injection and inductance estimation are carried out on γ-axis of fictitious γ–δ frame whose angle (θ_e) is assigned by the algorithm. By sweeping the θ_e, the whole rotor is scanned to obtain L_d and L_q values which is described in Fig. 3. Through incremental angle steps $(\Delta\,\theta_e)$, a scan of 180° is sufficient to find L_d and L_q.

A. Spatial Inductance Estimation

1) Basic Methodology: This section discusses how L_d and L_q are estimated without the knowledge of the initial rotor position. A sinusoidal high-frequency voltage is injected thorough γ-axis as given in (1), while δ-axis voltage is zero

$$v_\gamma = V_i \cos(\omega t + \alpha_v) \tag{1a}$$

$$v_\delta = 0. \tag{1b}$$

Then, the motor experiences the voltages in (2) on d- and q-axes. Here, θ_r is the unknown initial rotor position whereas θ_e is assigned by the proposed method during the spatial scanning process. Fig. 3 depicts these angles

$$v_d = V_\gamma \cos(\theta_e - \theta_r)\cos(\omega t + \alpha_v) \tag{2a}$$

$$v_q = V_\gamma \sin(\theta_e - \theta_r)\cos(\omega t + \alpha_v). \tag{2b}$$

These voltages force the currents given in (3). Here, stator resistance and inverter voltage distortion are momentarily ignored

$$i_d = \frac{V_\gamma}{\omega L_d}\cos(\theta_e - \theta_r)\cos(\omega t + \alpha_i) \tag{3a}$$

$$i_q = \frac{V_\gamma}{\omega L_q}\sin(\theta_e - \theta_r)\cos(\omega t + \alpha_i). \tag{3b}$$

Then, d–q frame currents in (3) are transformed back to γ–δ frame and i_γ in (4) is obtained. Here, the aim is to express the spatial inductance $L(\theta_e)$ in terms of L_d and L_q

$$i_\gamma = \left(\frac{\cos^2(\theta_e - \theta_r)}{L_d} + \frac{\sin^2(\theta_e - \theta_r)}{L_q}\right)\frac{V_\gamma}{\omega}\cos(\omega t + \alpha_i). \tag{4}$$

From (1a) and (4) and the assumption in (3), the spatial inductance may be analytically represented by (5). This implies a spatial inductance variation similar to Fig. 2 as the θ_e is swept from 0° to 360°

$$L(\theta_e) = \frac{1}{\left(\frac{\cos^2(\theta_e - \theta_r)}{L_d} + \frac{\sin^2(\theta_e - \theta_r)}{L_q}\right)}. \tag{5}$$

When $(\theta_e$–$\theta_r)$ is around 0° or 180°, the effective inductance at γ-axis becomes approximately L_d. Similarly, when $(\theta_e$–$\theta_r)$ is around 90° or 270°, L_q is the effective inductance seen from γ-axis. Hence, the proposed method spatially scans 180° through incremental angle steps $(\Delta\theta_e)$ as depicted in Fig. 3 and calculates the inductance at each angle step. After 180° search, the minimum calculated inductance is assigned to L_d and the maximum one is assigned to L_q. This approach guarantees that the actual d- and q-axes are inside the scanned area as shown in Fig. 2 and enables the whole auto-tuning process without knowing the initial rotor position.

2) Inductance Calculation: Inductance is estimated following each $\Delta\theta_e$ increments. As the sinusoidal injection is used, the inductance can be estimated by impedance relation given in (9). Here, the amplitudes and phases of γ-axis voltage and current are obtained from the Goertzel blocks in Fig. 5 and used in (9).

To derive (9), the injection voltage is decomposed into two parts; one being in phase with the resulting γ-axis current and the other being 90° phase shifted. Because of this phase relation, the first term is resistive voltage and the second part is an inductive voltage which is also expressed in (8). By equating (8) and the

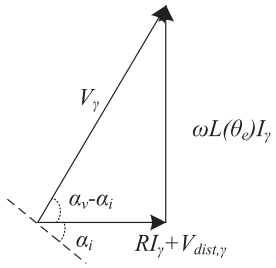

Fig. 4. Phasor representation of voltage components.

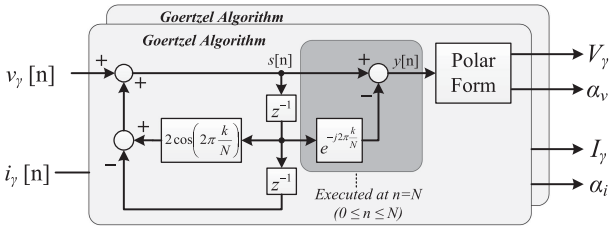

Fig. 5. Signal amplitude and phase detection with Goertzel algorithm.

second term of (7), the inductance expression is obtained in (9). This process can also be visualized using phasor in Fig. 4

$$i_\gamma = I_\gamma \cos(\omega t + \alpha_i) \tag{6}$$

$$v_\gamma = V_\gamma \cos(\alpha_v - \alpha_i)\cos(\omega t + \alpha_i) - V_\gamma \sin(\alpha_v - \alpha_i)\sin(\omega t + \alpha_i) \tag{7}$$

$$L(\theta_e)\frac{di_\gamma}{dt} = -L(\theta_e)\omega I_\gamma \sin(\omega t + \alpha_i) \tag{8}$$

$$L(\theta_e) = \frac{V_\gamma}{\omega I_\gamma}\sin(\alpha_v - \alpha_i). \tag{9}$$

Note that (9) uses $\sin(\alpha_v - \alpha_i)$ term to reject the resistive voltage of stator resistance and inverter voltage distortion from the inductance estimation. Note that the distortion voltage behaves as current-dependent nonlinear resistance [14]–[17] and in some cases, it can be more dominant than the stator resistance as a resistive term. Therefore, it is important to introduce this mitigation approach against the resistive effects for more accurate inductance measurements.

3) Signal Detection: Inductance estimation requires the amplitude and phase of the injected voltage and the resultant current. Thus, the signals are detected using DFT with Goertzel algorithm implementation, shown in Fig. 5 [18]. IIR part of the Goertzel algorithm is given in (10) which has v_γ or i_γ as input for $n = 0$ to $n = N - 1$. After executing the IIR part with zero input when $n = N$, FIR part is implemented as (11). Then, signal amplitude and angle are found by taking the polar form of the complex number $y[n]$. By means of this algorithm, measurement robustness and precision of DFT is achieved through low processing power and memory

$$s[n] = v_\gamma[n] + 2\cos\left(2\pi\frac{k}{N}\right)s[n-1] - s[n-2] \tag{10}$$

$$y[n] = s[n] - e^{-j\left(2\pi\frac{k}{N}\right)}s[n-1]. \tag{11}$$

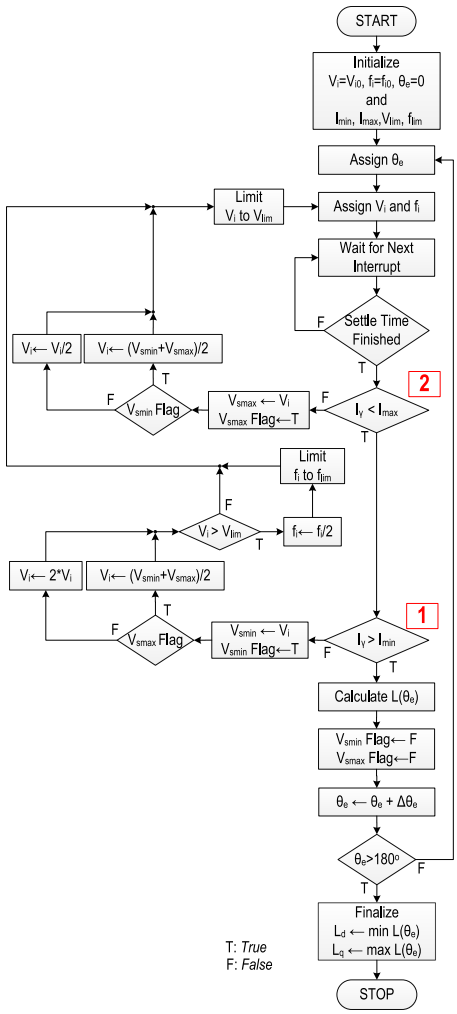

Fig. 6. Automated injected signal identification procedure.

B. Injection Voltage Amplitude and Frequency Selection

In practical application, the amplitude and frequency of the injection voltage are imperative due to the unknown parameters. Depending on the motor under test, the resultant current might be too low to provide meaningful information due to poor signal-to-noise ratio (SNR), or too high resulting in over-current fault. Therefore, the algorithm depicted in Fig. 6 automatically sets the appropriate injection signal amplitude and frequency. Basically, this algorithm searches suitable voltage and frequency pairs. In this way, an injection signal can successfully be selected.

1) Initialization of Voltage Amplitude and Frequency: Since the motor parameters are not known at this stage, initial values for injection voltage amplitude and frequency are critical. Hence, it is proposed to start with low initial voltage (V_{i0}) and high initial frequency (f_{i0}) so that initial motor current is minimized. Here, f_{i0} selection depends on sampling frequency. Naturally, it should be selected as high as possible to increase inductive impedance where the upper limit is the Nyquist frequency. At Nyquist frequency, the injected voltage becomes square wave because digitally controlled inverter behaves as

zero-order hold (ZOH). Since the square wave includes high harmonic content, the resulting current would have significant harmonic components beyond Nyquist frequency. Subsequently, sampling this distorted current would cause aliasing in the fundamental component. Therefore, it is suggested to select f_{i0} as one-tenth of the sampling frequency. This is also detailed in Section IV-B.

For V_{i0}, a value smaller than IGBT voltage drop can safely be selected as a simple guidance because the injection voltage should be higher than IGBT drop to cause current flow. However, V_{i0} can be selected much lower in the expense of short convergence-time penalty in the order of milliseconds. After selecting V_{i0}, (12) is used to cross-check the minimum motor inductance that can be measured at or below rated current

$$L_{\min} = \frac{V_{i0}}{2\pi f_{i0} I_{\text{rated}}}. \tag{12}$$

2) Voltage Amplitude and Frequency Search: After starting with a low and safe current level, the injection signal needs to be increased in order to enhance SNR through the algorithm in Fig. 6. The proposed approach defines a range, minimum ($I_{\min}$) and maximum current ($I_{\max}$) limits and then keeps the resulting current amplitude (I_γ) within these limits before calculating the inductance. The purpose of using $I_{\min}$ is to provide robust current measurement considering SNR and analog-to-digital converter bit size and avoid inductance measurement at very low current levels. $I_{\min}$ selection puts a limit for maximum motor inductance that can be measured which is expressed in the following equation:

$$L_{\max} = \frac{V_{\lim}}{2\pi f_{\lim} I_{\min}}. \tag{13}$$

If I_γ is outside the $I_{\min}$ and $I_{\max}$ interval, a correction action is executed at the nodes 1 and 2 in Fig. 6. In the first case, I_γ might be less than $I_{\min}$. If the current has never been higher than $I_{\max}$ during the inductance measurement at a given spatial angle (θ_e), then the voltage is simply doubled. But if the current has previously exceeded $I_{\max}$ ($V_{\text{smax}}Flag = T$), the injection voltage is selected as the average of the present voltage and V_{smax}. To narrow down the search interval from the upper side, V_{smax} is set to the voltage in which I_γ exceed $I_{\max}$.

In the second case, I_γ might be higher than $I_{\max}$. If the current has never been less than $I_{\min}$ during the inductance measurement at a given spatial angle (θ_e), then the voltage is simply halved. But if the current has previously gone below $I_{\min}$ ($V_{\text{smin}}Flag = T$), the injection voltage is selected as the average of the present voltage and V_{smin}. To narrow down the search area from the lower side, V_{smin} is set to the voltage which reduces I_γ less than $I_{\min}$. During the test, the realizable voltage is limited by dc-link voltage. Therefore, the proposed method puts a maximum voltage limit as $V_{\lim}$ which is defined in (14) representing the maximum achievable voltage in the linear pulsewidth modulation (PWM) region

$$V_{\lim} = \frac{V_{\text{dc}}}{\sqrt{3}}. \tag{14}$$

When the calculated voltage amplitude becomes higher than this voltage limit, the injection frequency is halved as illustrated in Fig. 7(b). Hence, motor impedance [$\sim \omega_i L(\theta_e)$] and the required minimum injection voltage [$\sim \omega_i L(\theta_e) I_{\min}$] decrease. The frequency is successively decreased until the current converges to the designated range between $I_{\min}$ and $I_{\max}$ or the minimum frequency limit is reached.

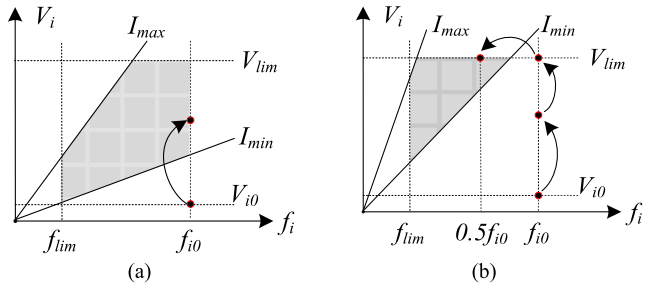

Fig. 7. Examples of injection signal automatic selection procedure. (a) Case 1: No frequency change. (b) Case 2: Frequency change.

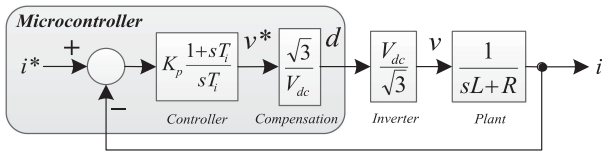

Fig. 8. Current loop model.

To illustrate how the algorithm works, two examples are given in Fig. 7. The grey areas represent the allowed convergence points of injection voltage amplitude and frequency. In the first case, the initial current is below $I_{\min}$; therefore, the voltage is increased and then the algorithm converges. In the second case, possibly because of higher machine impedance and/or the lower dc-link voltage, the algorithm converges only after hitting $V_{\lim}$ and then decreasing the frequency.

III. Controller Tuning

This paper uses model-based controller tuning. The current loop model is shown in Fig. 8 where V_{dc} is used as compensation in the controller to neutralize the dc-link voltage variation and its effect on loop gain. For simplicity, only one axis current controller is visualized.

In the literature, there are various approaches to tune the current controller. One of them is to design a controller in a continuous domain using well-known methods such as symmetrical optimum and then discretize it [19]. On the other hand, other methods for direct discrete-domain design are also proposed especially for the cases with low sampling number per fundamental period [20], [21]. Once the inductance values are in hand, obviously the user is free to select and customize any tuning method. This paper uses a relatively simple method to merely demonstrate the effectiveness of the proposed auto-tuner. Using the estimated L_d and L_q values, the self-commissioning algorithm automatically tunes the current controller, given the phase margin of θ_{pm} and loop cross-over frequency of ω_c. The delay due to digital control may be compensated by selecting a higher phase margin. Ignoring the resistance, the open-loop transfer

function (OLTF) is given in (15). Accordingly, the proportional-integral (PI) controller gains of K_p (proportional gain) and T_i (integration time constant) are calculated as (16) and (17)

$$\text{OLTF}\,(s=j\omega) \cong \frac{K_p}{L}\frac{\sqrt{1+\omega^2 {T_i}^2}}{\omega^2 T_i} e^{j\left(\tan^{-1}(\omega T_i)-\pi\right)} \quad (15)$$

$$T_i = \frac{\tan\theta_{\text{pm}}}{\omega_c} \quad (16)$$

$$K_p = \omega_c L \sin\theta_{\text{pm}}. \quad (17)$$

IV. Practical Considerations

A. Transient Currents Due to Voltage Injection

Sinusoidal voltage application to motors results in sinusoidal steady-state and transient current components. Because motor resistance and inductance are not known in advance, die-out time for the transient is unknown. To illustrate this argument, a generalized sinusoidal voltage of (18) is applied to an inductive load with power factor angle of φ at the frequency of ω_i, given in (19). Assuming zero initial current, the closed form current response is provided in (20)

$$v_\gamma(t) = V_\gamma \cos(\omega_i t + \alpha_v) \quad (18)$$

$$\varphi = \tan^{-1}\left(\frac{\omega_i L(\theta_e)}{R}\right) \quad (19)$$

$$i_\gamma(t) = \frac{V_i}{\sqrt{R^2+(\omega_i L(\theta_e))^2}} \left[\cos\left[\omega_i t-(\varphi-\alpha_v)\right]-\cos(\varphi-\alpha_v)\, e^{-\frac{R}{L(\theta_e)}t}\right]. \quad (20)$$

If the amplitude of transient current with decaying exponential form in (20) is significant and it lasts longer, it can disturb the detection of the sinusoidal current amplitude and phase. Therefore, it is proposed to choose the phase of the injected voltage (α_v) as zero in order to minimize the transient current and provide fast settling at steady-state. In this way, the $\cos(\varphi–\alpha_v)$ term in (20) becomes negligible because the power factor (φ) in (19) approaches to 90° under high-frequency injection. However, as φ is not exactly 90°, for higher performance, the paper chooses to insert a certain number of the period for settling. The experiment part uses two periods for settling, then the next period is used in DFT measurement. In addition, DFT-based signal detection helps to reject the effect of transient current because DFT selects only the injection frequency with its bandpass effect. If the voltage and/or frequency updates of the algorithm in Fig. 6 are executed at the end of a fundamental injection period, the whole test benefits from this minimized transient current.

B. Digital Control Effects on Voltage Synthesis and Current Sampling

As a voltage synthesis tool, inverter behaves as ZOH because it is digitally controlled. ZOH introduces delay and magnitude distortion. Because of this, the motor experiences a different voltage than the commanded one. This phenomenon is

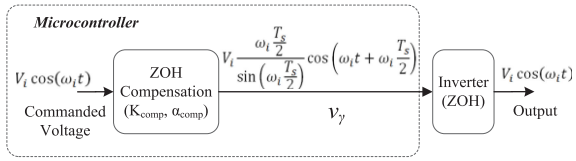

Fig. 9. Compensation for inverter ZOH effect.

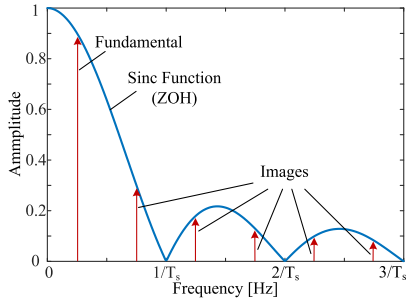

Fig. 10. Generated image components due to ZOH.

pronounced more at high frequencies which is the case for the proposed method. To solve this issue, gain and phase behavior of ZOH [22] should be considered which is given in (21) where T_s is sampling time

$$H_{\text{ZOH}}(\omega) = \frac{\sin\left(\omega\frac{T_s}{2}\right)}{\omega\frac{T_s}{2}} e^{-j\omega\frac{T_s}{2}}. \quad (21)$$

It is preferred that the distortion due to ZOH be rectified in the software. The gain and phase compensation should be applied to the voltage reference in the controller as shown in (22) and Fig. 9

$$v_\gamma(t) = K_{\text{comp}} V_i \cos(\omega_i t + \alpha_{\text{comp}}) \quad (22a)$$

$$K_{\text{comp}} = \frac{\omega_i \frac{T_s}{2}}{\sin\left(\omega_i \frac{T_s}{2}\right)} \quad (22b)$$

$$\alpha_{\text{comp}} = \omega_i \frac{T_s}{2}. \quad (22c)$$

Another issue related to digital control is aliasing. Due to its ZOH nature, the inverter generates the fundamental voltage and also its images around the multiples of sampling frequency as illustrated in Fig. 10. When the compensation in (22) is applied; the voltage realized by the inverter can be formulated as in (23) which includes harmonics due to ZOH. Here, N is the sample number per injection period. Assuming pure inductive load for simplicity, the resultant current is given in (24). When the injection frequency approaches to Nyquist frequency, the harmonic currents due to ZOH become significant. Then, these harmonic currents cause considerable aliasing after sampling the motor currents as given in (25). Aliasing on the fundamental component is especially critical because Goertzel algorithm selects only this frequency. To solve this issue, this paper limits the maximum injection frequency to one-tenth of the sampling

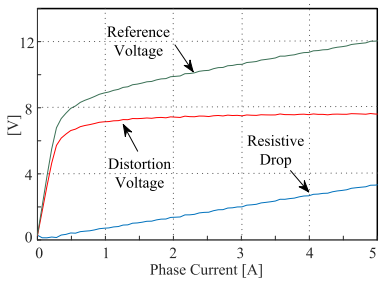

Fig. 11. Inverter voltage distortion characteristics.

frequency so that the aliasing effect is minimized

$$V_{\gamma,\text{motor}}(t) = V_i\left\{1\cos(\omega_i t) - \frac{1}{N-1}\cos((N-1)\omega_i t) + \frac{1}{N+1}\cos((N+1)\omega_i t) - \frac{1}{2N-1}\cos((2N-1)\omega_i t)\cdots\right\} \tag{23}$$

$$i_{\gamma,\text{motor}}(t) = \frac{V_0}{\omega_i L(\theta_e)}\left\{1\sin(\omega_i t) - \left(\frac{1}{N-1}\right)^2 \sin((N-1)\omega_i t) + \left(\frac{1}{N+1}\right)^2 \sin((N+1)\omega_i t) - \left(\frac{1}{2N-1}\right)^2 \sin((2N-1)\omega_i t)\cdots\right\} \tag{24}$$

$$i_{\gamma,\text{sampled}}(t) = \frac{V_i}{\omega_i L(\theta_e)}\left\{1 + \left(\frac{1}{N-1}\right)^2 + \left(\frac{1}{N+1}\right)^2 + \left(\frac{1}{2N-1}\right)^2\cdots\right\}\sin(\omega_i t). \tag{25}$$

C. Inverter Voltage Distortion

Dead-time, gate signal delays, and power semiconductors contribute to the inverter voltage distortion [14]–[17]. To illustrate distortion characteristics, the inverter phase voltage from the test setup used in this paper is shown in Fig. 11 as a function of phase current. The inverter distortion is experimentally obtained by storing the reference voltages for steady-state dc current values, while the current is regulated at several dc points between 0 and 5 A. As pointed out in [14]–[17] and also understood from Fig. 11, the distortion voltage behaves as a current-dependent nonlinear resistor.

Overall system model in γ-axis becomes as given in (26) when the inverter distortion is included. The distortion voltage referred to γ-axis is given in (27) where $V_{\text{dist}}(i_{a/b/c})$ is the distortion voltage due to phase currents (i_a, i_b, and i_c)

$$v_\gamma = Ri_\gamma + L(\theta_e)\frac{di_\gamma}{dt} + v_{\text{dist},\gamma} \tag{26}$$

$$v_{\text{dist},\gamma} = \frac{2}{3}\left[V_{\text{dist}}(i_a)\cos(\theta_e) + V_{\text{dist}}(i_b)\cos\left(\theta_e - \frac{2\pi}{3}\right) + V_{\text{dist}}(i_c)\cos\left(\theta_e - \frac{4\pi}{3}\right)\right]. \tag{27}$$

The block diagram of this model including the distortion voltage effects on the motor is depicted in Fig. 12.

Although the inverter voltage distortion alters the dynamics as given in (26), the proposed method eliminates its effects on the inductance measurement in two ways:

1) the resistive nature of the distortion voltage is avoided by explicitly considering the phase angle difference between voltage and current as in (9), instead of assuming 90° phase (pure inductive load) due to high frequency;
2) harmonic effects due to the nonlinear shape of the distortion voltage are also avoided by only considering the injection-frequency components via DFT. Notice that the proposed method does not use dead-time compensation or identify the distortion characteristics. Instead, it algorithmically rejects the distortion voltage effects in parameter estimation.

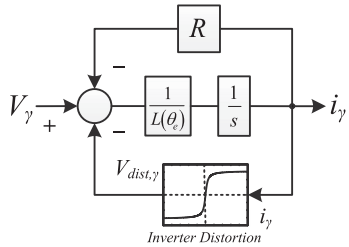

Fig. 12. Inverter voltage distortion effect on the actual motor voltage.

TABLE I
SYSTEM PARAMETERS

Motor power	1.5 hp
Dc-link voltage	300 V
Base frequency	100 Hz
Base current	10 A
Switching freq.	10 kHz
Dead-time	2 µs
I_{min}	0.5 A.
I_{max}	5 A
V_{i0}	0.02 V
f_{i0}	1 kHz
Settle time	2 periods
$\Delta\theta_e$	1 degree

V. EXPERIMENTAL RESULTS

Several experiments are carried out to verify the proposed method using the system in Table I. The control structure is summarized in Fig. 13 and the physical test setup is shown in Fig. 14.

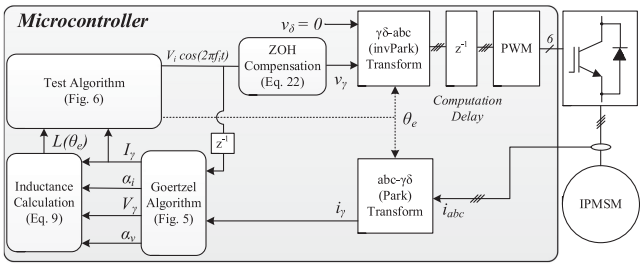

Fig. 13. Block diagram of the experimental system.

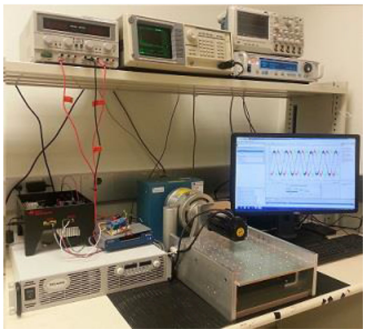

Fig. 14. Test setup.

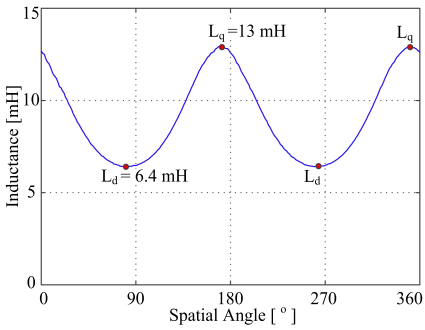

Fig. 15. Experimental result for spatial inductance mapping.

A. Spatial Inductance Map

The proposed method scans the motor by measuring the inductance at discrete spatial angle points, incremented by 1 electrical degree. Although the algorithm is developed to scan 180°, in this part, the whole rotor is scanned to better visualize the performance. The spatial inductance map result of the test motor described in Table I is given in Fig. 15. L_d and L_q are compared to the ones obtained by a reference current-injecting self-commissioning method detailed in [3]. Here, L_d and L_q are estimated as 6.4 mH and 13.0 mH, respectively, where the reference method yields 6.3 mH and 12.9 mH as given in Table II.

B. Auto-Tuned Current Loop: Dynamic Performance

Sinusoidal reference tracking and step response performances are provided in Fig. 16. Following the inductance estimation, the control firmware automatically tunes the PI controller using (16) and (17). The cross-over frequency (ω_c) and phase margin

TABLE II
VERIFICATION OF THE ESTIMATED PARAMETERS

	IPMSM		SPMSM	BLDC	SynRM		IM
(mH)	L_d	L_q	L_s	L_s	L_d	L_q	L_σ
Proposed	6.4	13.0	8.8	19	155	56	49
Reference	6.3	12.9	8.5	19.5	157	58	48
Difference	1.5%	0.8%	3.5%	2.5%	1.3%	3.5%	2%

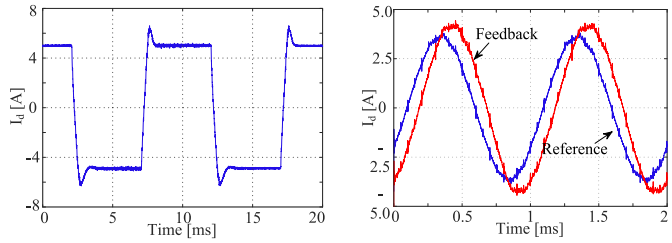

Fig. 16. Performance of auto-tuned current loop: Step reference (left) and sinusoidal reference (right) tracking.

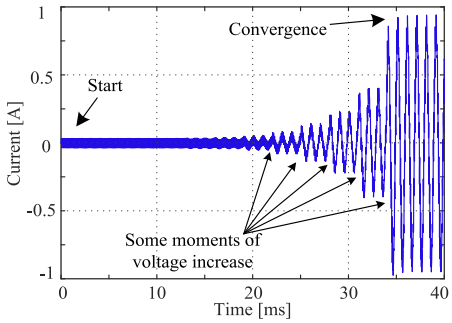

Fig. 17. Phase–A current: The safe start-up of the proposed method.

$(\theta_{\rm pm})$ are selected as 0.8 kHz and 60°, respectively. It is apparent that the auto-tuned current loop is stable. It can track a 1-kHz sinusoidal reference with approximately 40° phase delay and its settling time is approximately 1 ms for step reference changes.

C. Start-Up Without Over-Current Fault

Safe start-up is proven by showing the initial voltage search process in Fig. 17.

The algorithm starts at 1 ms and it converges to a suitable voltage at 37 ms. The voltage is increased 12 times to satisfy 0.5–A $I_{\rm min}$ requirement. Each measurement time includes 3 periods of injection (2 for settling and 1 for DFT). The voltage is initialized as 0.02 V which causes negligible current flow initially. But, due to the geometric increase in the injection voltage amplitude, the algorithm safely converges to a suitable voltage value in a short time without causing the over-current fault.

D. Immunity Against the Inverter Voltage Distortion

The inverter distortion voltage is more influential at lower frequencies because inductive voltage drop decreases with frequency while the distortion voltage stays more or less constant.

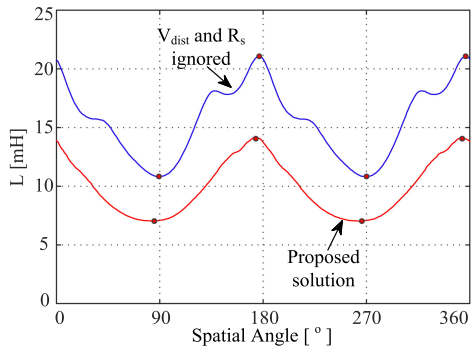

Fig. 18. Immunity against inverter voltage distortion at low injection frequency.

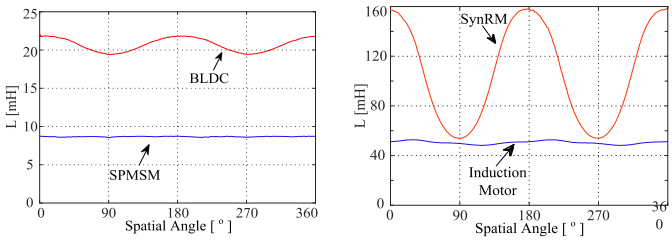

Fig. 19. Application of the proposed method in BLdc, SPMSM (left), and SynRM, IM (right).

Therefore, in order to better visualize the immunity of the proposed method against inverter voltage distortion, the initial value of the injection frequency (f_{i0}) is decreased to 100 Hz here. The spatial inductance estimation result is given in Fig. 18. The first case calculates the inductance using $L(\theta_e) = \frac{V_\gamma}{(2\pi f_i) I_\gamma}$ and hence, ignores stator resistance and distortion voltage and assumes the pure inductive load. Therefore, when the distortion voltage is comparable to inductive voltage, erroneously higher inductances are estimated. The second curve in Fig. 18 is the proposed solution of (9) which considers the signal phase angles to reject the resistive and distortion drops from the estimation. It gives almost the same result as Fig. 15 and proves the immunity against inverter distortion effects.

E. Application to Other Motor Types

Although the proposed method is discussed mainly for IPMSM, it can be applied to other motor types as well. This makes it a candidate of universal current-loop auto-tuner aimed for self-commissioning. For verification, a brushless dc (BLdc) motor and a surface-mounted PMSM (SPMSM) are examined as shown in Fig. 19. SPMSM is a 9–slot, 8–pole design and it does not show any saliency. On the other hand, the BLdc motor has a slight saliency although its datasheet does not give detail on spatial inductance variation. Furthermore, induction (IM) and synchronous reluctance motors (SynRM) are also tested and the spatial variations of IM leakage inductance (L_σ) and SynRM inductance are provided in Fig. 19. Since only L_σ is limiting the current transients, it is the relevant inductance for current loop tuning in IM. Therefore, only L_σ is considered here, rather than magnetizing inductance. Furthermore, q-axis flux of SynRM has a unique feature that differential L_q is relatively higher around zero current until a little current saturates the thin iron bridges in the rotor. Therefore, to obtain nominal L_q value of SynRM, a little more current should be there in the test. This translates into higher $I_{\min}$ selection when applying the proposed method to SynRM.

The estimated values of the proposed method are compared to the ones obtained by a current-injecting self-commissioning [3]. The comparative results for all tested motors are given in Table II. In order to avoid repetition, the current controller performances of these machines are not given here. Overall, this result shows that the proposed method can be applied to practically all ac motors.

For nonsalient motors, the spatial scanning can be opted out because spatial scanning generally is not necessary due to non-saliency. This may decrease the test time slightly. In this case, inductance estimation is done at only one spatial angle such as $\theta_e = 0$.

VI. Conclusion

This paper presented a complete solution for current loop auto-tuning as the first step of self-commissioning procedure which is essential for sensorless IPMSM drives. The proposed method accurately measured the motor d- and q-axis inductances which were then used to obtain the desired dynamic response of the current controllers through a simple tuning approach. There were a number of superiorities of the proposed method. First, it utilizes an open-loop voltage injection method and hence eliminates the need for the feedback controller during inductance estimation. The injection amplitude and frequency were selected automatically less than 100 ms without causing any disruption in the system. Second, it did not need the initial rotor position detection or physical alignment of the rotor to a known angle, and hence agnostic to initial position. Third, the parameter estimation in the suggested approach was not affected by the inverter voltage distortion. Also, its successful application to different machine types showed that the proposed method is a strong candidate to be universal current loop auto-tuner for commercial motor drive self-commissioning.

References

[1] J.-I. Ha, K. Ide, T. Sawa, and S.-K. Sul, "Sensorless rotor position estimation of an interior permanent-magnet motor from initial states," *IEEE Trans. Ind. Appl.*, vol. 39, no. 3, pp. 761–767, May/Jun. 2003.

[2] L. M. Gong and Z. Q. Zhu, "Robust initial rotor position estimation of permanent-magnet brushless AC machines with carrier-signal-injection-based sensorless control," *IEEE Trans. Ind. Appl.*, vol. 49, no. 6, pp. 2602–2609, Nov./Dec. 2013.

[3] S. Morimoto, M. Sanada, and Y. Takeda, "Mechanical sensorless drives of IPMSM with online parameter identification," *IEEE Trans. Ind. Appl.*, vol. 42, no. 5, pp. 1241–1248, Sep./Oct. 2006.

[4] D. Tadokoro, S. Morimoto, Y. Inoue, and M. Sanada, "Method for auto-tuning of current and speed controller in IPMSM drive system based on parameter identification," in *Proc. Int. Power Electron. Conf.*, 2014, pp. 390–394.

[5] S. A. Odhano, P. Giangrande, R. I. Bojoi, and C. Gerada, "Self-commissioning of interior permanent-magnet synchronous motor drives with high-frequency current injection," *IEEE Trans. Ind. Appl.*, vol. 50, no. 5, pp. 3295–3303, Sep./Oct. 2014.

[6] S. A. Odhano, R. Bojoi, S. G. Rosu, and A. Tenconi, "Identification of the magnetic model of permanent-magnet synchronous machines using DC-biased low-frequency AC signal injection," *IEEE Trans. Ind. Appl.*, vol. 51, no. 4, pp. 3208–3215, Jul./Aug. 2015.

[7] G. Wang, L. Qu, H. Zhan, J. Xu, L. Ding, G. Zhang, and D. Xu, "Self-commissioning of permanent magnet synchronous machine drives at standstill considering inverter nonlinearities," *IEEE Trans. Power Electron.*, vol. 29, no. 12, pp. 6615–6627, Dec. 2014.
[8] N. Nomura and S. Higuchi, "Auto-tuning method of inductances for permanent magnet synchronous motors," in *Proc. Int. Power Electron. Conf.*, 2014, 1522–1528.
[9] S.-M. Yang and K.-W. Lin, "Automatic control loop tuning for permanent-magnet AC servo motor drives," *IEEE Trans. Ind. Electron.*, vol. 63, no. 3, pp. 1499–1506, Mar. 2016.
[10] Y.-S. Lai and M.-H. Ho, "Self-commissioning technique for high bandwidth servo motor drives," in *Proc. Energy Convers. Congr. Expo.*, pp. 342–347, Sep. 2017.
[11] P. Mattavelli, L. Tubiana, and M. Zigliotto, "Simple control autotuning for PMSM drives based on feedback relay," in *Proc. Eur. Conf. Power Electron. Apps*, 2005, pp. 1–10.
[12] K. Astrom and T. Hagglund, "Automatic tuning of simple regulators with specifications on phase and amplitude margins," *Automatica*, vol. 20, pp. 645–651, 1984.
[13] J.-S. Yoon, K.-G. Lee, J.-S. Lee, and K.-B. Lee, "Off-line parameter identification of permanent magnet synchronous motor using a Goertzel algorithm," *J. Elect. Eng. Technol.*, vol. 10, no. 6, pp. 2262–2270. Nov. 2015.
[14] A. Cichowski and J. Nieznanski, "Self-tuning dead-time compensation method for voltage-source inverters," *IEEE Power Electron. Lett.*, vol. 3, no. 2, pp. 72–75, Jun. 2005.
[15] Y. Park and S.-K. Sul, "A novel method utilizing trapezoidal voltage to compensate for inverter nonlinearity," *IEEE Trans. Power Electron.*, vol. 27, no. 12, pp. 4837–4846, Dec. 2012.
[16] G. Shen *et al.*, "Automeasurement of the inverter output voltage delay curve to compensate for inverter nonlinearity in sensorless motor drives," *IEEE Trans. Power Electron.*, vol. 29, no. 10, pp. 5542–5553, Oct. 2014.
[17] N. Bedetti, S. Calligaro, and R. Petrella, "Self-commissioning of inverter dead-time compensation by multiple linear regression based on a physical model," *IEEE Trans. Ind. Appl.*, vol. 51, no. 5, pp. 3954–3964, Sep./Oct. 2015.
[18] A. V. Oppenheim and R. W. Schafer, *Discrete-Time Signal Processing*, 3rd ed. Upper Saddle River, NJ, USA: Pearson, 2010, pp. 745–748.
[19] V. Blasko and V. Kaura, "A new mathematical model and control of a three-phase AC–DC voltage source converter," *IEEE Trans. Power Electron.*, vol. 12, no. 1, pp. 116–123, Jan. 1997.
[20] H. Kim, M. W. Degner, J. M. Guerrero, F. Briz, and R. D. Lorenz, "Discrete-time current regulator design for AC machine drives," *IEEE Trans. Ind. Appl.*, vol. 46, no. 4, pp. 1425–1435, Jul./Aug. 2010.
[21] M. Hinkkanen, H. A. A. Awan, Z. Qu, T. Tuovinen, and F. Briz, "Current control for synchronous motor drives: Direct discrete-time pole-placement design," *IEEE Trans. Ind. Appl.*, vol. 52, no. 2, pp. 1530–1541, Mar./Apr. 2016.
[22] J. Proakis and D. G. Manolakis, *Digital Signal Processing – Principles, Algorithms, and Applications*, 3rd ed. Upper Saddle River, NJ, USA: Prentice-Hall, 1996, pp. 765–768.

Feyzullah Erturk was born in Karaman, Turkey. He received the B.S. and M.S. degrees in electrical engineering from Middle East Technical University, Ankara, Turkey, in 2012 and 2015, respectively. He is currently working toward the Ph.D. degree in electrical engineering with the University of Texas at Dallas, Richardson, TX, USA.

He is currently working with Delphi Technologies, Kokomo, IN, USA, on the control of electric motors for electric vehicles (EV)/hybrid electric vehicles (HEV) applications. Previously, he was an Engineer with Aselsan Inc., Ankara, Turkey, and a Research Assistant with the University of Texas at Dallas. His research interests include design, control, and self-commissioning of electric motor drives.

Bilal Akin (S'03–M'08–SM'13) received the Ph.D. degree in electrical engineering from the Texas A&M University, College Station, TX, USA, in 2007.

He was an R&D Engineer with Toshiba Industrial Division, Houston, TX, USA, from 2005 to 2008. From 2008 to 2012, he worked as an R&D Engineer at C2000 DSP Systems, Texas Instruments, Houston, TX. Since 2012, he has been with University of Texas at Dallas as faculty.

Dr. Akin is recipient of NSF CAREER'15 award, IEEE IAS Transactions 1st Place Prize Paper Award and Top Editors Recognition Award from IEEE TVT Society, Jonsson School Faculty Research Award and Jonsson School Faculty Teaching Award. He is an Associate Editor of IEEE TRANSACTIONS ON INDUSTRY APPLICATIONS and IEEE TRANSACTIONS ON VEHICULAR TECHNOLOGY. His research interests include design, control and diagnosis of electric motors & drives, digital power control and management, fault diagnosis & condition monitoring of power electronics components and ac motors.